

# We are IntechOpen, the world's leading publisher of Open Access books Built by scientists, for scientists

6,900

Open access books available

186,000

International authors and editors

200M

Downloads

Our authors are among the

154

Countries delivered to

TOP 1%

most cited scientists

12.2%

Contributors from top 500 universities



WEB OF SCIENCE™

Selection of our books indexed in the Book Citation Index  
in Web of Science™ Core Collection (BKCI)

Interested in publishing with us?  
Contact [book.department@intechopen.com](mailto:book.department@intechopen.com)

Numbers displayed above are based on latest data collected.  
For more information visit [www.intechopen.com](http://www.intechopen.com)



# Exhaust Gas Heat Recovery for an ORC: A Case Study

*Armando Gallegos-Muñoz, Fabián Luna-Cabrera,  
Martín Picón-Núñez, Francisco Elizalde-Blancas  
and Juan Manuel Belman-Flores*

## Abstract

This work aims at developing a heat exchanger (HEX) sizing approach considering the need to maximize the heat recovery within the limitations of pressure drop and space. The application consists in the recovery of the energy contained in exhaust gases coming from an internal combustion engine (ICE). Two heat exchanger geometries are selected as case studies. The design approach involves the application of design of experiments (DOE) techniques and computational fluid dynamics (CFD) simulations. DOE techniques are used to observe the influence of some selected parameters (factors) in the design of the heat exchangers, and CFD simulations are carried out to determine the performance of the heat exchanger. The information obtained is used to determine local Nusselt number correlations that are used for the design of the heat exchangers.

**Keywords:** heat exchanger, heat waste, CFD, neural network, optimization

## 1. Introduction

Industrial applications of waste heat recovery require several types of heat exchangers. The correct selection and optimization of the heat exchangers are critical for heat transfer. Several papers have been published that deal with the selection of the most suitable heat exchanger technology for a specific application. Hatami et al. [1] developed a numerical study to model two types of heat exchangers (HEXs) used to recover the exhaust waste heat from internal combustion engines (ICEs). In the work, authors aimed at finding the best viscous model to fit experimental data. One of the exchangers belongs to a compression ignition (CI) engine with water as cold fluid, while the second exchanger belonged to a spark ignition (SI) engine with a mixture of 50% water and 50% ethylene glycol (EG) as cold fluid. From the study, authors concluded that the heat recovery can be improved by increasing the number of fins and length, where maximum heat recovery occurs with high engine load and speeds. On a different work, Hatami et al. [2] applied a response surface methodology (RSM) based on central composite design (CCD) to derive an optimization approach of finned-type heat exchangers to recover waste heat from the exhaust of a diesel engine. The design is performed for a single-point operation (1600 rpm and 60 N m) of an OM314 diesel engine. Based on the CCD principle, 15 exchangers with different fin heights (FH), fin numbers,

and fin thicknesses (FT) were numerically modeled, and optimization was carried out to maximize heat recovery and minimize pressure drop along the heat exchanger. The results showed that the height of the fins has a higher impact on pressure drop than fin number and thicknesses. On the other hand, fin number enhances heat recovery.

Bari et al. [3] performed a study on pancake-shaped heat exchangers to be fitted in a vehicle. The heat exchangers studied were of the shell-tube and U-tube type. CFD simulations were carried out to optimize the design and calculate the additional power that could be achieved by using these optimized heat exchangers. The effectiveness of pancake-shaped heat exchanger is on average 3% higher than that of the optimized round-shaped heat exchanger. Bari et al. [4] conducted experiments using water as the working fluid to estimate the exhaust waste heat recoverable from a diesel engine using two available heat exchangers. Two identical shell and tube heat exchangers were fitted into the exhaust of the engine, and experiments were conducted to estimate the additional energy that could be gained with this setup. Simulation tools were used to compare the performance of the heat exchangers with experimental data. Then the effects of changing important parameters such as length, diameter of shell, and number and diameter of tubes on the heat recovery were investigated. It was found that the effectiveness was higher for smaller shell diameters. After optimization, the additional power increased from 16 to 23.7%.

Tan et al. [5] reported the use of artificial neural network (ANN) models to simulate the thermal performance of a compact fin-tube heat exchanger with air and water/ethylene glycol antifreeze mixtures as the working fluids. They demonstrated that, once trained, an artificial neural network could predict the overall heat transfer rate between the liquid and air streams with a high degree of accuracy. The neural network predictions were in much closer agreement to the experimental data than corresponding predictions derived using a conventional nonlinear regression model.

Shivakumar et al. [6] tested the applicability of neural networks in order to correlate the experimentally determined heat transfer parameters of a multi-pass cross-flow heat exchanger. The waste heat from an internal combustion (IC) engine was used to heat the water in a cross-flow heat exchanger. The experimental results were used to train the ANN model. A multilayer perceptron (MLP) with back-propagation algorithm was used for training the network. The predicted results by the ANN model were compared with experimental data. They concluded that an MLP network can be used to predict the thermal performance characteristics of multi-pass cross-flow heat exchanger using a limited number of experimental data.

Hatami et al. [7] used a multi-objective optimization approach based on ANN and genetic algorithm (GA) to the numerical outcomes of a finned-tube heat exchanger in a diesel exhaust heat recovery application. The results confirm that the optimized case widely increased the recovered heat and exergy while keeping the pressure drop at low levels. Although the optimized case exhibited higher irreversibility, its second law efficiency is significantly greater than the non-optimized case, especially at high engine loads. The average efficiency of the proposed HEX is about 8% for the exergy recovery from the exhaust of a light diesel engine.

Aly et al. [8] investigated the 3D turbulent flow and heat transfer of coiled tube-in-tube heat exchangers. Heat exchangers are analyzed considering conjugate heat transfer from the hot fluid in the inner-coiled tube to the cold fluid in the annulus region. After simulations, the Taguchi method was used to find the optimum condition for some design parameters in the range of coil diameter from 0.18 to 0.3 m and tube and annulus flow rates from 2 to 4 and 10 to 20 l/min, respectively. Results showed that the Gnielinski correlation (used extensively for predicting Nusselt number for turbulent flow in ducts) can be used to predict Nusselt number for both the inner-coiled tube and the annular coiled tube using the friction factor correlation

for helical tubes. The application of the Taguchi method showed that the annulus side flow rate, the tube side flow rate, the coil diameter, and the flow configuration are the most important design parameters in coiled tube-in-tube heat exchangers.

Hossain et al. [9] optimized heat exchangers used in the recovery of exhaust heat from a 40-kW diesel generator. With the available experimental data, computer simulations were carried out to optimize the design of the heat exchangers. The optimized heat exchangers were then used to estimate additional power gained considering the turbine isentropic efficiency. The proposed heat exchangers could produce 11% additional power using water as the working fluid at a pressure of 15 bar. The effects of the working fluid pressure were also investigated to maximize the additional power production. The pressure was limited to 15 bar which was constrained by the exhaust gas temperature. However, higher pressure is possible for higher exhaust gas temperatures from higher capacity engines.

This work aims at showing a stepwise approach for the sizing of a heat exchanger for waste heat recovery and subsequent use in an Organic Rankine Cycle (ORC). For maximum power production and minimum pressure drop, the exchanger must be optimized. Besides, space limitation poses an additional constraint to the design. The approach introduced in this work allows the designer to simultaneously achieve all these design objectives.

## **2. Method description**

The proposed method seeks to maximize heat transfer and minimize pressure drop. Besides, within the exchanger, overheated areas (to avoid evaporation of the cold fluid) and overcooled areas (to avoid condensation and corrosion on the hot side) must also be minimized [10]. A combination of different tools is used to solve the complex problem. To avoid overdesign, accurate Nusselt correlation must be developed. Given the space limitations, two exchanger geometries, namely, a finned heat exchanger and a helical heat exchanger, are analyzed to have an additional degree of freedom between heat recovery and pressure drop. For the same heat load, the finned tube will exhibit lower heat transfer area but higher pressure drop, while the helical tube will have larger surface area but lower pressure drop. Given the constraints in terms of mass flow rate, pressure drop, heat transfer, and space, maximum and minimum values for these parameters must be fixed. Since a very large possible combination of operating conditions can result, it is important to discriminate between them. One way of doing this is by designing the experiments or identifying the most representative set of design variables that allow to reduce the search space. Once this is done, in principle the geometry should be constructed and tested to see which of the designs exhibit overheating and overcooling areas. Computational fluid dynamics techniques can be used to this end. Besides, CFD can also provide local heat transfer coefficients which can be correlated for design purposes. As mentioned earlier, the approach used in this work is by means of artificial neural networks.

Since maximum power production is the final desired outcome, the design with the maximum exergy recovery will lead to maximum power production. Thus, exergy analysis is included, and the Organic Rankine Cycle is modeled using the HYSYS simulator [11].

### **2.1 Process description**

The steps followed in the analysis introduced in this work are detailed described below and graphically shown in **Figure 1**.

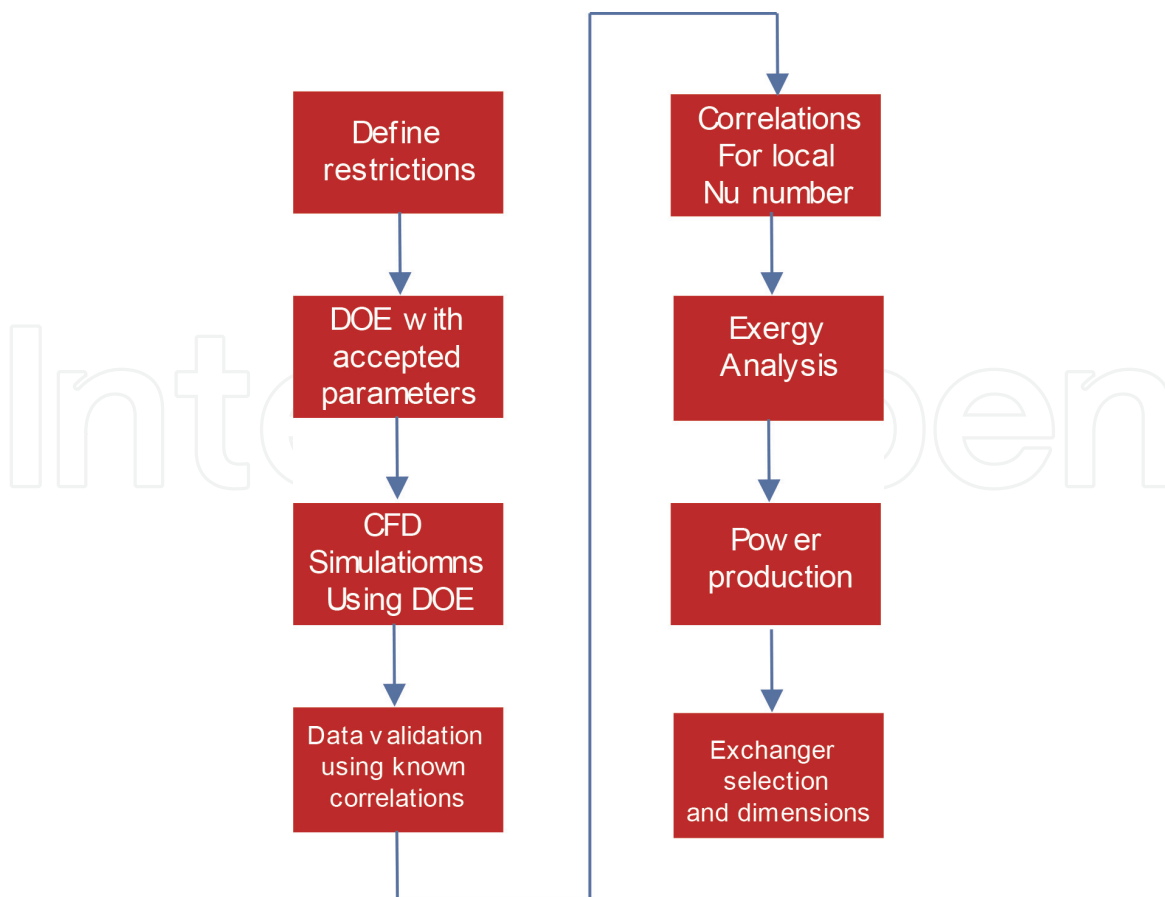


**Figure 1.**  
*Sequence of the proposed analysis and design method.*

1. The restriction parameters (mass flow rate, pressure drop, heat transfer, power required, and geometrical constraints) are defined.
2. A design of experiments, [12] is established using the parameters (factors: heat flux, pressure drop, overheated and overcooled areas of both types of heat exchangers) accepted to select the conditions for the CFD simulation.
3. A CFD simulation for each of the resulting experiments above is carried out.
4. Local Nusselt numbers obtained from the CFD simulations are compared with published correlations for validation.
5. Once the results of the simulation are validated, these can be used to produce regression equations to predict the best combination of parameters to maximize heat transfer and minimize overheated and overcooled areas and pressure drop.
6. The neural network developed in [10] is used to fit complex relation emerging from CFD results.
7. Exergy analysis is applied to determine the exergy gain and exergy efficiency of the heat exchangers.
8. The heat recovered from the diesel engine is used in an Organic Rankine Cycle for power production.

## 9. Selection and design of final heat exchanger.

The diagram of the process is presented in **Figure 1**.

## 3. Case study

The proposed method is applied on two types of heat exchangers, namely, a finned-tube heat exchanger and a helical-tube heat exchanger. These configurations were selected because they are compact, of relatively simple geometry and of easy modification of parameters. The open literature indicates that these types of heat exchangers are typically used in heat recovery from exhaust gases. The geometry of both exchangers consists of two concentric tubes: the hot gas flows at the internal tube and ethylene glycol flows in the annular space between tubes. The outer surface of the exchangers is isolated. **Figures 2** and **3** show the helical-tube heat exchanger and the finned-tube heat exchanger, respectively. The only parameter that remains the same, as reference, for both types of heat exchangers is the linear length from inlet to outlet which is set to 1 m.

CFD techniques are used to analyze the performance of the units. The response variables of the CFD simulation are gas outlet pressure (PG), ethylene glycol outlet pressure (PEG), heat exchanger's surface area referred to the hot side (AG), heat exchanger's surface area referred to the cold side (AEG), heat flux from the hot side (QG"), and heat flux to the cold side (QEG"). For the design of experiments, the factors considered for the case of the helical-tube heat exchanger are internal

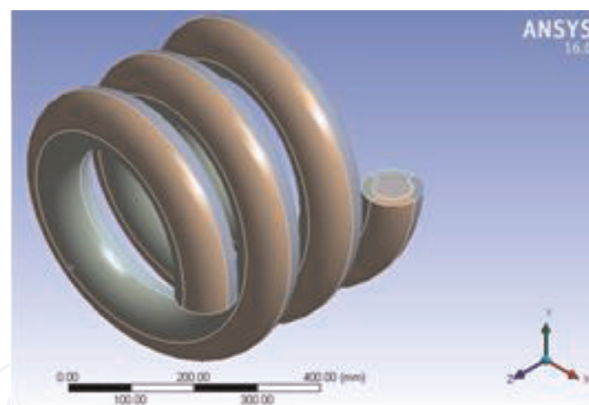


**Figure 2.**  
*Helical-tube heat exchanger.*

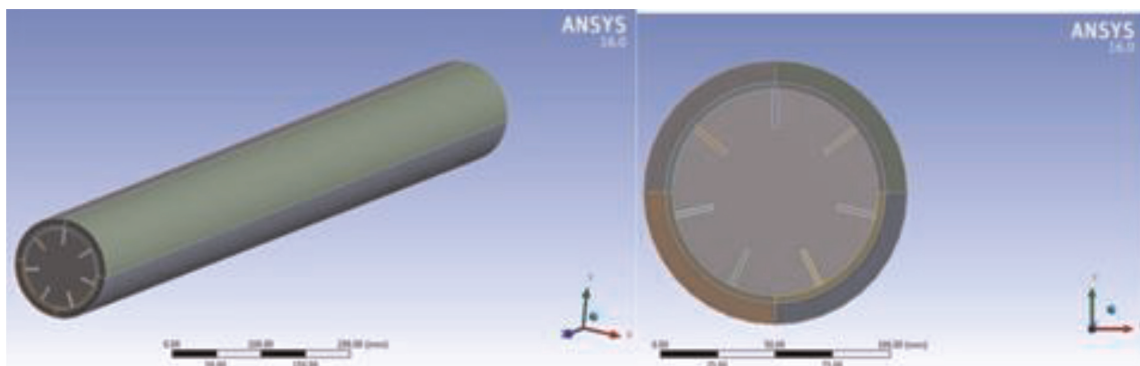


**Figure 3.**  
*Finned-tube heat exchanger.*

diameter (ID), external diameter (ED), mass flow rate of the gas (mass), and inlet gas temperature (temp). The range of parameters are shown in **Table 1**.

In the case of the finned-tube heat exchanger, where the fins are assumed to be straight, the parameters considered are fin height, fin thickness, fin density (FD), mass ratio between gas and ethylene glycol (mass ratio), and inlet gas temperature (temp). The range of the parameters are shown in **Table 2**.

The variables were selected based on the impact they have on the dimensions of the heat exchanger, as well as on the operating conditions over the range where maximum heat transfer will be achieved. These variables will allow to find the optimal conditions of the heat exchanger when determining new correlations for the Nusselt number to eliminate the risk of oversizing.

The factors chosen for the finned heat exchanger were taken from the work of Hatami et al. [7]. The mass ratio factor is the ratio between the two fluids, namely, gas and ethylene glycol. After trying different mass ratios, the best fit between CFD results and Minitab [13] regressions was obtained. To select the factors for the case of helical heat exchanger, six parameters were initially considered: internal diameter, external diameter, helix diameter, helix pitch, mass of gas, and temperature of gas. Some parameters were eliminated to get the minimum number of factors that could exhibit a good fitting to the simulated results. The parameters eliminated were helix diameter and helix pitch. The minimum number of factors required to get a good fit were internal diameter, external diameter, and temperature and mass of gas.

The experiment design indicates that 27 configurations to simulate the helical-tube heat exchanger are needed, while 46 are required for the finned-tube unit. Each one of these configurations was simulated using Ansys Fluent 2016 [14]. The simulations were made under the following considerations:

- a. The standard  $k-\epsilon$  model with standard wall function turbulent model was used for the gas side.
- b. A laminar model was used at the ethylene glycol side ( $50 \leq Re \leq 250$ ).

Parameter	Low	High
ID [mm]	60	80
ED [mm]	100	110
Mass [kg/s]	0.07	0.135
Temp [K]	550	700

**Table 1.**  
*Design parameters for the helical-tube heat exchanger.*

Parameters	Low	High
FH [mm]	17	32
FT [mm]	2	6
FD [mm]	4	10
Mass ratio	0.5	0.71
Temp [K]	550	700

**Table 2.**  
*Design parameters for the finned-tube heat exchanger.*

- c. There is no phase change on either side.
- d. The gas pressure drop must be lower than 10 kPa.
- e. The  $y_+$  value must be around  $y_+ > 30$  and  $y_+ < 300$  (wall treatment) [15].

The density of the gas was determined using the incompressible ideal gas model because the Mach number in all cases was lower than 0.3. The density and viscosity of ethylene glycol were calculated using a user-defined function (UDF). In this way, the variation of density and viscosity with temperature was considered applying the equations

$$\rho_{EG} = -0.9904 * temp + 1417 \quad (1)$$

$$\eta_{EG} = 3.724E4 \exp(-0.05021 * temp) + 0.2811 \exp(-0.01356 * temp) \quad (2)$$

For the thermal conductivity and viscosity of the hot gas, the equations used are

$$\kappa_{GA} = 6.22 * 10^{-5} * temp + 0.008116 \quad (3)$$

$$\eta_{GA} = 3.755 * 10^{-5} * \exp(0.0002586 * temp) - 3.561 * 10^{-5} * \exp(-0.001614 * temp) \quad (4)$$

To validate the results of the CFD simulations, the following published correlations are used [10]:

Helical-tube heat exchanger  
 Turbulent regime

$$Nu_s = \frac{PrRe(f_s/8)}{1 + 12.7\sqrt{\frac{f_s}{8}}(Pr^{\frac{2}{3}} - 1)} \left[ 1 + \left(\frac{d_h}{L}\right)^{2/3} \right] \quad (5)$$

Laminar regime

$$Nu = \left[ \left( 4.364 + \frac{4.636}{x_3} \right) + 1.816 \left( \frac{De}{x_4} \right)^{3/2} \right]^{1/3} \quad (6)$$

Finned-tube heat exchanger  
 Turbulent regime

$$\frac{Nu_n}{Nu_{D-n}} = \left[ \frac{d_i}{d_{im}} \left( 1 - \frac{2e}{d_i} \right) \right]^{-0.2} \left( \frac{d_i d_h}{d_{im}^2} \right)^{0.5} \sec^3 \beta \quad (7)$$

Laminar regime

$$Nu = 1.86 \left( \frac{Pe_b d_i}{L} \right)^{1/3} \left( \frac{\mu_b}{\mu_w} \right)^{0.14} \quad (8)$$

To determine the maximum exergy recovery, the expression used is

$$\frac{d\phi_{CV}}{dt} = \sum \dot{\phi}_Q + \sum \dot{m}_i \psi_i - \sum \dot{m}_e \psi_e + \dot{W}_{act} - \dot{I}_{total} \quad (9)$$

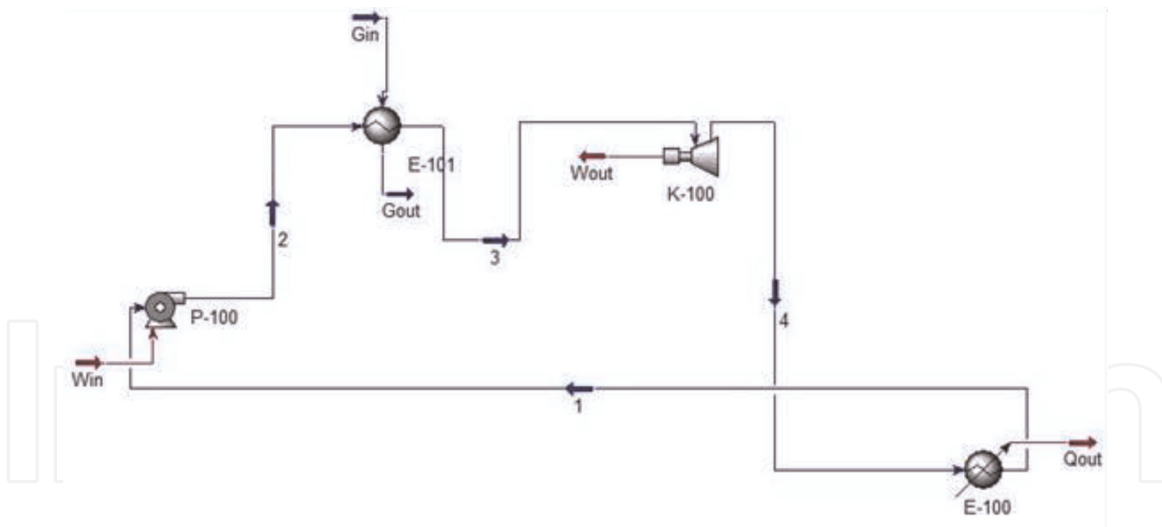


**Figure 4.**  
Flow diagram for the simulation of the organic Rankine cycle.

The generation of power from a low temperature heat source can be achieved by means of an Organic Rankine Cycle. **Figure 4** shows the diagram of the ORC cycle used for the simulation using HYSYS [11]. The working fluid is butane and the main components of the cycle are:

Pump (P-100): adiabatic efficiency 75%.

Heat exchanger (heater) (E-101): tube passes 2, shell passes 1,  $\Delta P = 0$ .

Turbine (K-100): adiabatic efficiency 75%.

Heat exchanger (cooler) (E-100):  $\Delta P = 0$ .

## 4. Results

As described in the methodology applied (**Figure 1**), the first step consists in the validation of the CFD simulations according to the DOE results from where the input data are chosen. Next, from the CFD local Nusselt numbers obtained, correlations are obtained. Then an exergy analysis is applied to the heat exchangers, and finally the simulation in Aspen HYSYS [11] is carried out.

### 4.1 Validation of CFD simulation

For the CFD simulation, the sweep hex elements were used; 473,600 elements were applied to the helical-tube heat exchanger and 949,500 to the finned-tube heat exchanger. The boundary conditions used in the CFD simulations for both types of heat exchangers are inlet mass flow, outlet pressure and insulated external surface. The regime of flow is subsonic. The gas side exhibits turbulent flow and the ethylene glycol a laminar regime.

For the gas side, the conditions at the inlet are mass, temperature, turbulent intensity, and turbulent length scale. The conditions at the outlet are backflow temperature, turbulent intensity, and turbulent length scale. For the ethylene glycol side, the conditions at the inlet are mass and temperature. The CFD solution provides the following results for both exchangers: mean temperature, wall temperature, pressure drop, and heat flux.

For the grid independence, several meshes were tested for each of the 73 configurations; a total of 198 simulations were carried out with the aim of finding the meshes that exhibit less variation in the prediction of results. A finer mesh was used

at the inner face of the gas cavity, around the fins and at the inner and outer face of ethylene glycol cavity to fulfill the required  $y^+$  value. **Figures 5** and **6** show the refinement for the two types of heat exchangers. The parameters used in the solver of the CFD simulations are shown in **Table 3**.

The parameters in **Table 3** gave the best results regarding mass and energy balance. For turbulent flow, the physical model SIMPLEC is recommended [16]. For gradient, the least squares cell-based method was selected. This method is less expensive in terms of simulation time [17]. For pressure interpolation, the second-order scheme is recommended. Second-order upwind was used to get more accuracy in the solution of the momentum equations [18]. First-order upwind was used to calculate turbulent kinetic energy because it is less time-consuming [17]. First order upwind was used to calculate turbulent dissipation rate because it is less time consuming [17]. Second-order upwind was used to get more accuracy in the solution of the energy equations [18].

The results obtained from the CFD simulations were validated using Eqs. (5)–(8). **Figures 7–10** show the comparison of Nusselt number. It can be observed that, for both heat exchanger geometries, the numerical results and the ones obtained from the correlation show similar tendency with a good approximation between them.

In the same way, local Nusselt number for both types of heat exchangers is presented in **Figures 11–14**. The most relevant configurations (experiments) were considered for each type of heat exchanger.

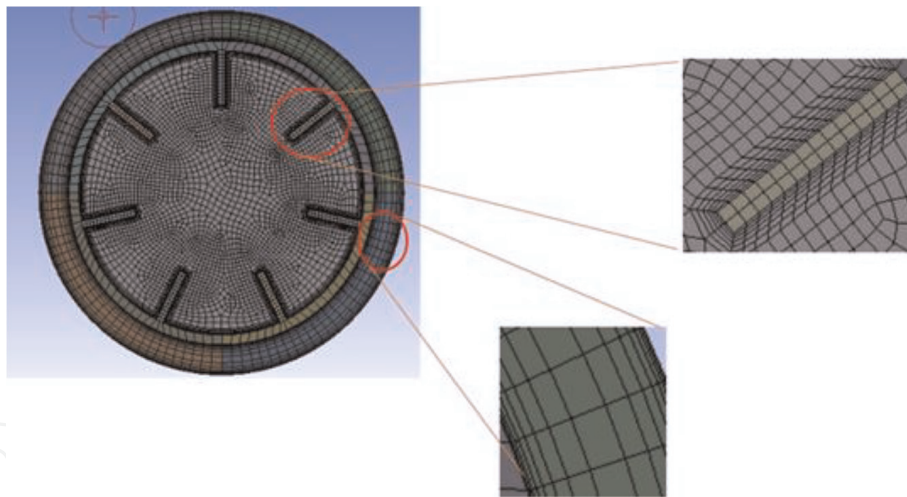


**Figure 5.**  
*Mesh refinement in the finned-tube geometry.*

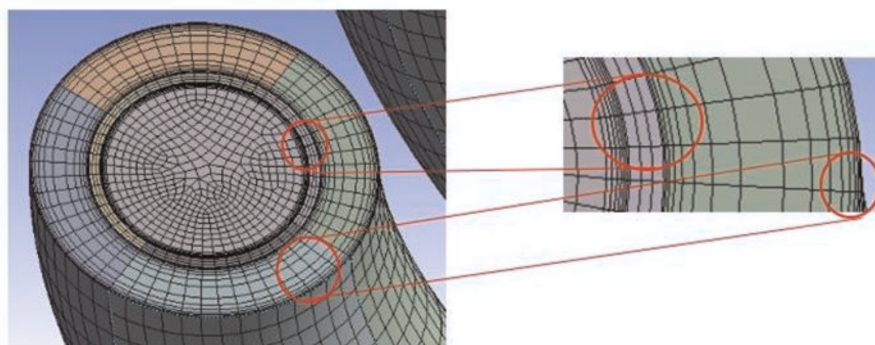


**Figure 6.**  
*Mesh refinement in the helical-tube geometry.*

## 4.2 Design of experiments (DOE)

With the aim of obtaining regression equations for Nu number, the design of experiments is applied. A second-order regression model for each of the variables is used. The DOE used was the Box-Behnken response surface design. The advantages of this method are as follows: it is a second-order model, and the experimental

Time	Steady
Scheme	SIMPLEC
Gradient	Least squares cell-based method
Pressure	Second order
Momentum	Second-order upwind
Turbulent kinetic energy	First-order upwind
Turbulent dissipation rate	First-order upwind
Energy	Second-order upwind

**Table 3.**  
Parameters used in the solver of the CFD simulations.

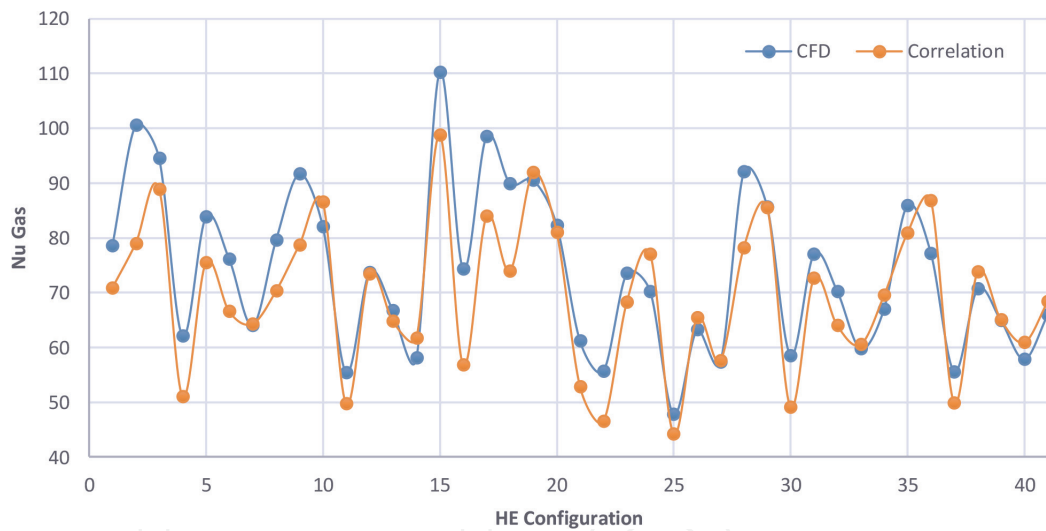


**Figure 7.**  
Validation of nu number on the hot side (G) for the finned-tube geometry.

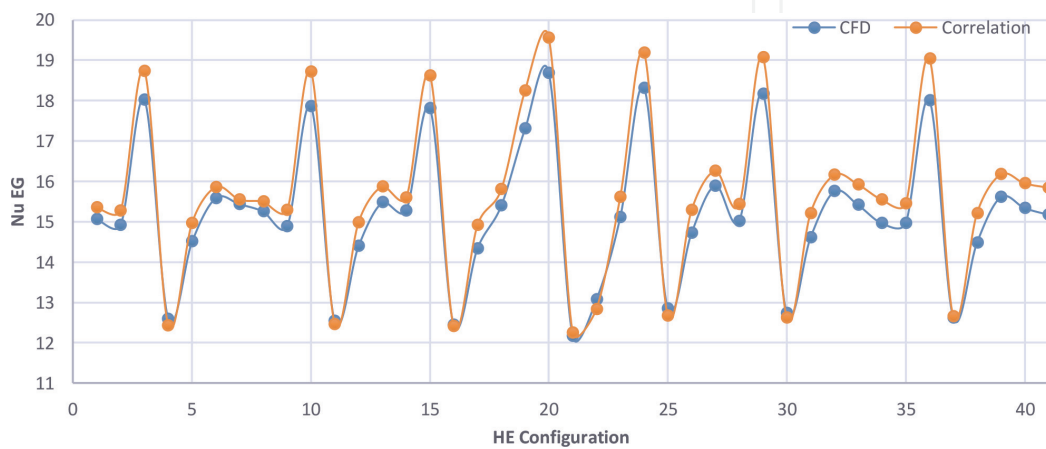


**Figure 8.**  
Validation of nu number on the cold side (EG) for the finned-tube geometry.

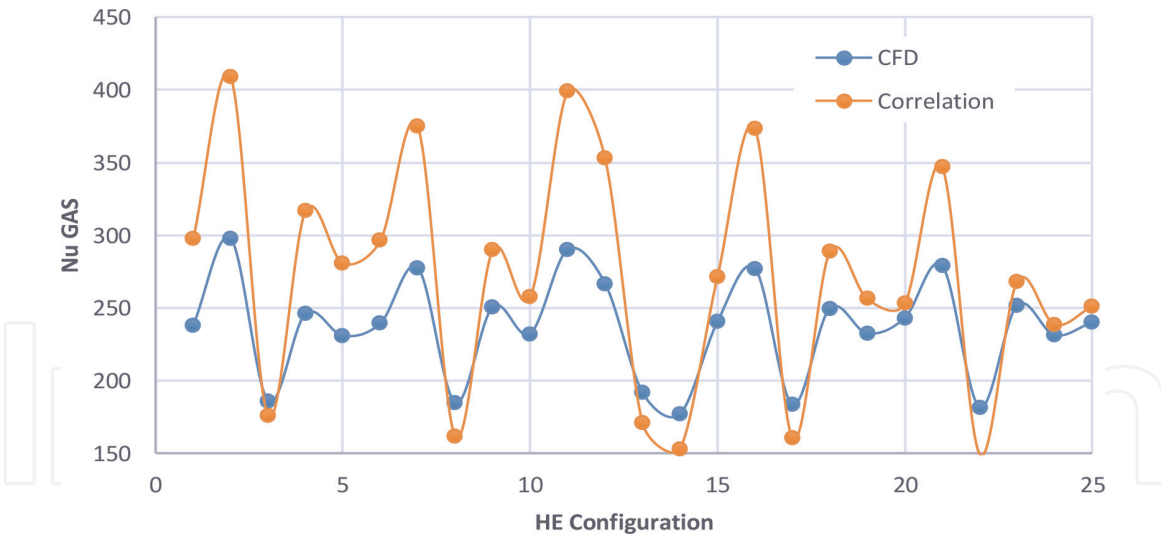


**Figure 9.**  
 Validation of nu number on the hot side (G) for the helical-tube geometry (G).

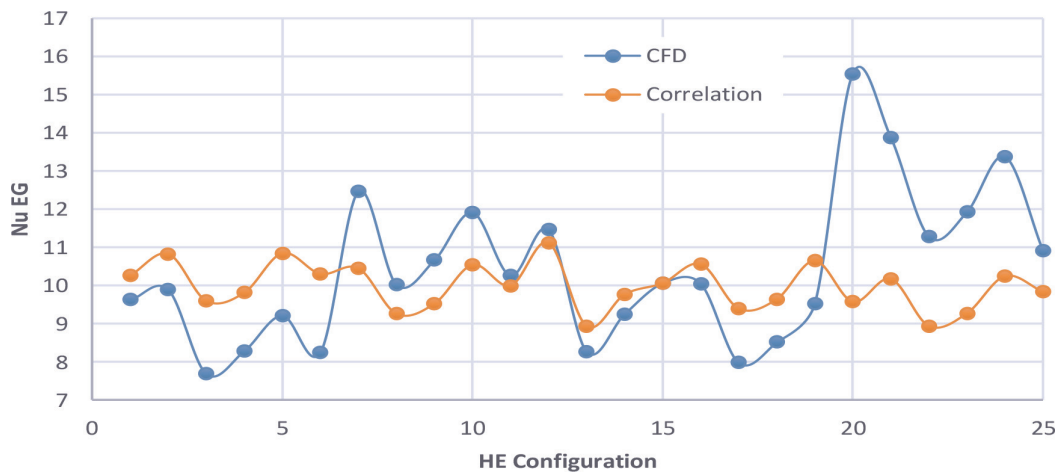


**Figure 10.**  
 Validation of nu number on the cold side (EG) for the helical-tube geometry.

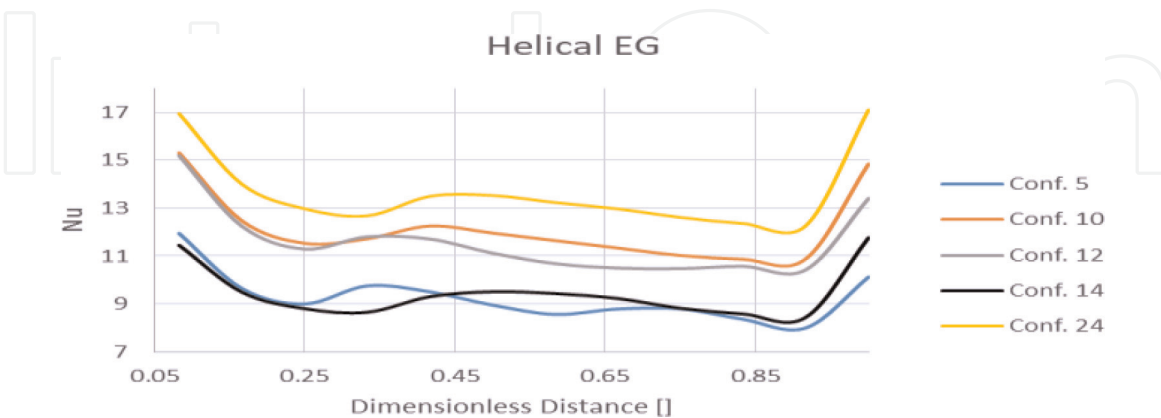


**Figure 11.**  
 Local Nusselt number for ethylene glycol side. Helical heat exchanger.

points are within the experimental space. Other methods like CCD have experimental points outside the experimental space which present divergence in the CFD simulations. Therefore, the Box-Behnken method was used in the computer simulations. The results are:

- a. Regression equations that relate inputs of each heat exchanger with the listed response variables
- b. Optimization plots which give the best parameter combination that maximizes some selected parameters and minimizes the rest of the parameters

The equations obtained are

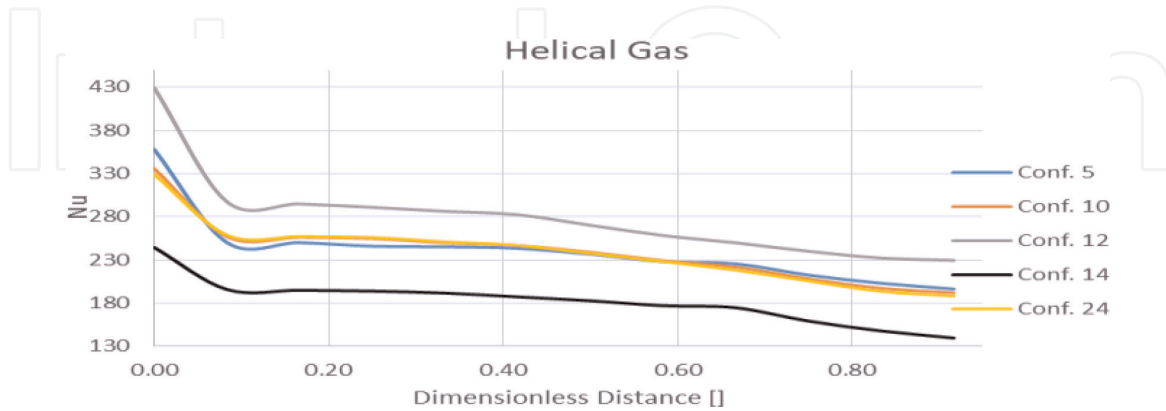


**Figure 12.**  
Local Nusselt number for gas side. Helical heat exchanger.

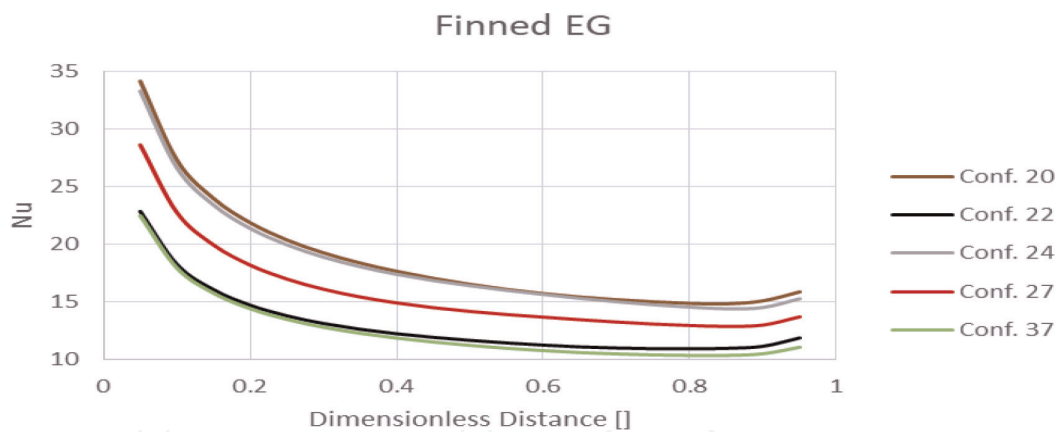


**Figure 13.**  
Local Nusselt number for ethylene glycol side. Finned heat exchanger.

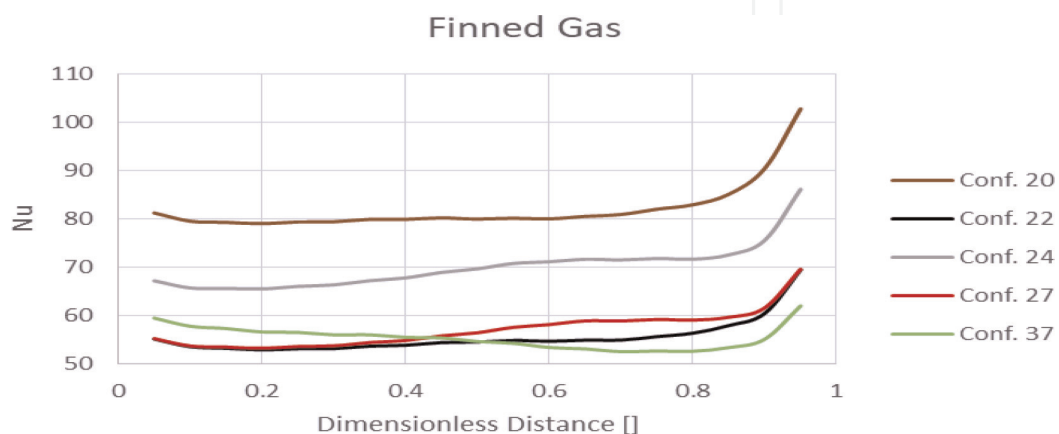


**Figure 14.**  
Local Nusselt number for gas side. Finned heat exchanger.

$$\begin{aligned}
 QG'' = & -19483 - 63ID - 92ED + 38412MASS + 86.9TEMP + 3.354ID^2 \\
 & + 2.66ED^2 - 3.20ID * ED - 0.164ID * TEMP - 658ED * MASS \quad (10) \\
 & - 0.471ED * TEMP + 225MASS * TEMP
 \end{aligned}$$

$$\begin{aligned}
 QEG'' = & -16212 - 111ED + 29547MASS + 73TEMP + 2.9ID^2 \\
 & + 2.59ED^2 - 3.22ID * ED - 0.131ID * TEMP - 585ED * MASS \quad (11) \\
 & - 0.403ED * TEMP + 212.9MASS * TEMP
 \end{aligned}$$

$$\begin{aligned}
 PEG = & 84 + 12.31ID - 9.4ED + 186MASS + 0.0657ID^2 + 0.0955ED^2 \\
 & - 0.000053TEMP^2 - 0.1834ID * ED + 4.39ID * MASS - 0.00292ID \\
 & * TEMP - 3.49ED * MASS + 0.00238ED * TEMP - 0.093MASS * TEMP \quad (12)
 \end{aligned}$$

$$\begin{aligned}
 PG = & 5.52 - 0.1187ID + 0.058ED + 26.86MASS + 0.00319TEMP \\
 & + 0.000386ID^2 - 0.000328ED^2 + 0.000157ID * ED - 0.000014ID \\
 & * TEMP + 0.00058MASS * TEMP \quad (13)
 \end{aligned}$$

$$\begin{aligned}
 AG = & 227 + 4.84ID - 2.05ED - 647MASS - 0.688TEMP + 0.02127ID^2 \\
 & + 0.0092ED^2 + 588.4MASS^2 + 0.000430TEMP^2 - 0.03658ID \\
 & * ED - 4.608ID * MASS - 0.004547ID * TEMP + 3.26ED * MASS \\
 & + 0.00300ED * TEMP + 0.6390MASS * TEMP \quad (14)
 \end{aligned}$$

Variable	S	R-sq	R-sq (adjusted)
QG	189.525	99.91	99.8
QEG	178.049	99.91	99.8
PG	0.0264185	99.93	99.86
PEG	4.01934	92.72	84.22
AG	0.924692	99.09	98.03
AEG	3.31958	98.23	95.3

**Table 4.** Standard deviation and mean square error for the case of the helical-tube geometry.

Variable	S	R-sq	R-sq (adjusted)
QG	101.885	99.89	99.81
QEG	180.39	99.92	99.85
PG	3.23035	99.43	98.74
PEG	0.110461	99.98	99.96
AG	0.242708	95.76	92.37
AEG	1.40149	99.12	98.42

**Table 5.** Standard deviation and mean square error for the case of the finned-tube geometry.

$$\begin{aligned}
 AEG = & -2184 - 5.78ID + 15.3ED + 259MASS + 4.686TEMP - 0.0198ID^2 \\
 & - 0.0837ED^2 - 1329MASS^2 - 0.003373TEMP^2 + 0.0611ID * ED \\
 & + 0.00095ID * TEMP - 1.37ED * MASS - 0.00121ED * TEMP \\
 & + 0.573MASS * TEMP
 \end{aligned}
 \tag{15}$$

Tables 4 and 5 show the parameters that have a significant effect as well as the standard deviation(s) and mean square error (R) for the helical and finned geometries.

From the regression parameters, it is evident that the heat flux on the gas side (QG”) and the heat flux on the ethylene glycol side (QEG”) for both types of heat exchangers have a high standard deviation. However, the regressed expressions for these parameters seem to adjust very well with the results of CFD simulations as shown in Figures 15–18. The legend RS fitting stands for response surface fitting.

The curves for the gas side and ethylene glycol side for the case of helical heat exchanger show a similar behavior since the distance separating both gas side and

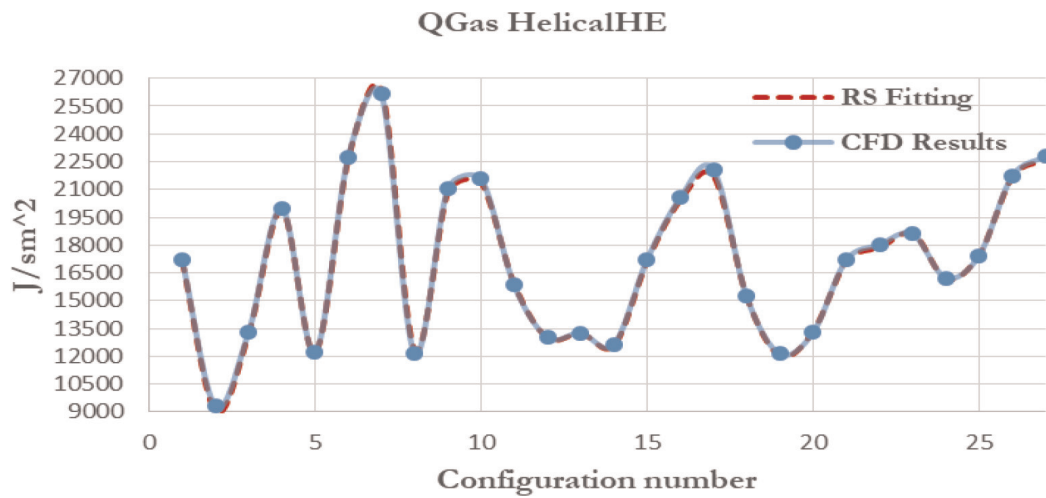


Figure 15. Plot of QG” vs. exchanger configuration for the helical-tube geometry.

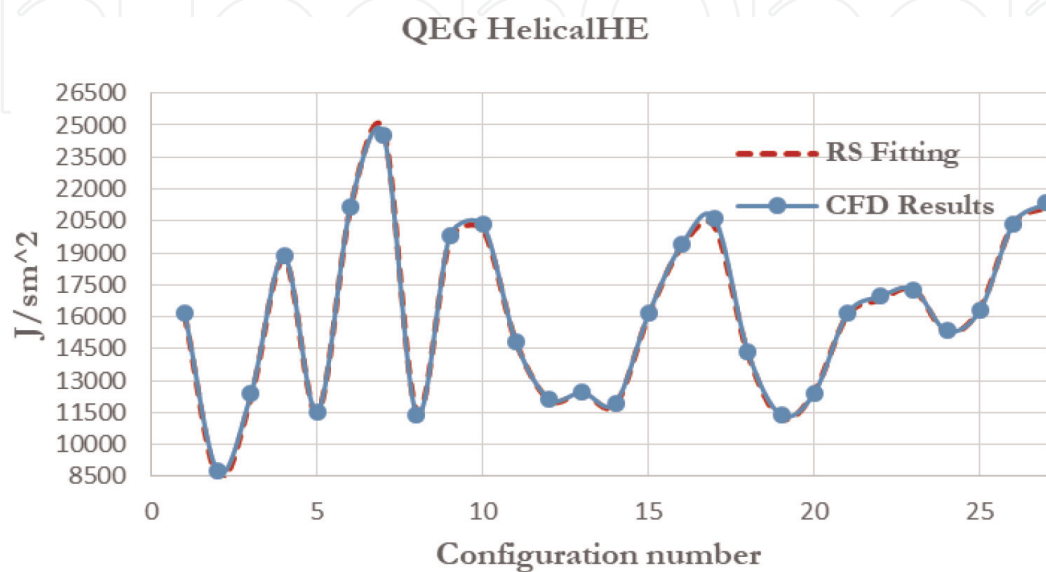
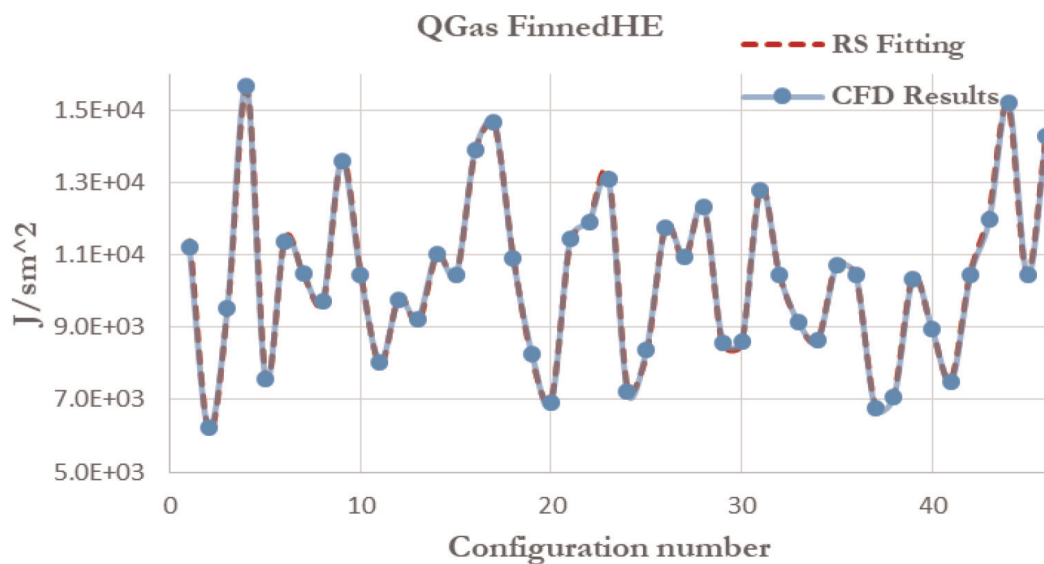


Figure 16. Plot of QEG” vs. exchanger configuration for the helical-tube geometry.

ethylene glycol side is small. This length corresponds to the inner tube thickness. So, the heat transfer area for the gas side and the ethylene glycol is similar. However, a difference in value exists between  $Q_G''$  and  $Q_{EG}''$ , and that difference can be observed in **Figures 15** and **16**.

In the case of the finned heat exchanger, the surface area of the gas side differs from that of ethylene glycol side. In this case the  $Q_G''$  and  $Q_{EG}''$  plots show a different behavior. This is shown in **Figures 17** and **18**.

In order to generate correlations for local Nusselt numbers exclusively for the bank of heat exchangers simulated, each one of the heat exchangers was divided in sections using the software Fluent [14]. These sections represent dimensionless distance from 0.05 to 0.95. In this way local Nusselt number can be obtained. The helical type of each exchanger was divided in 13 sections, and the finned type of each exchanger was divided in 19 sections. These divisions were done on each of the 41 configurations of the helical heat exchangers and 25 configurations of the finned heat exchangers. **Figure 19** shows the section on each heat exchanger.



**Figure 17.**  
Plot of  $Q_G''$  vs. exchanger configuration for the finned-tube geometry.

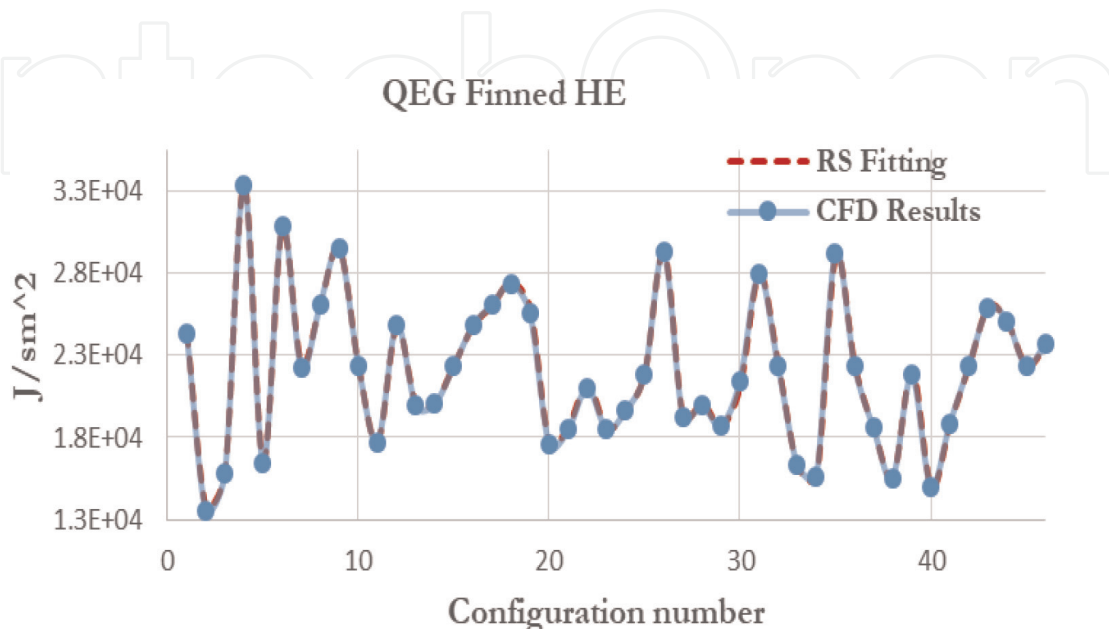
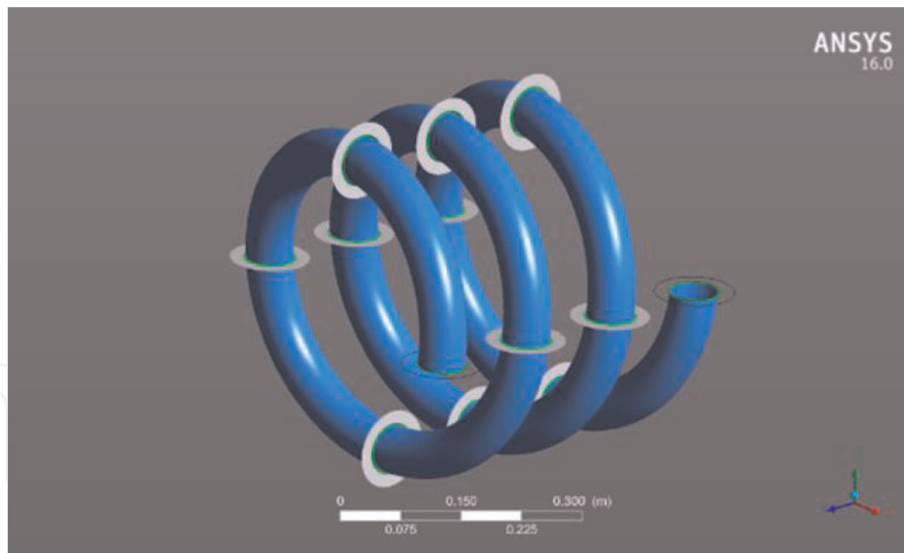
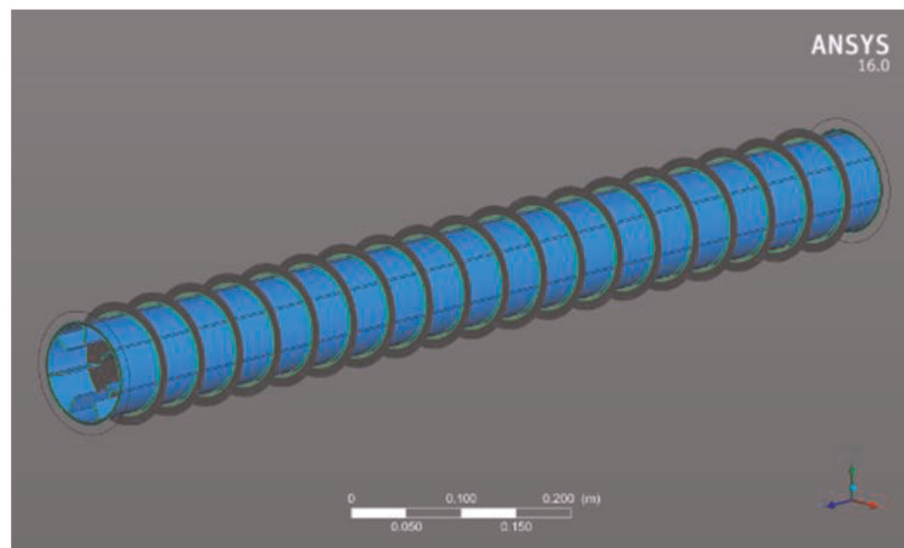


**Figure 18.**  
Plot of  $Q_{EG}''$  vs. exchanger configuration for the finned-tube geometry.



(a)



(b)

**Figure 19.** Section for the determination of the local nu number. (a) Helical heat exchanger and (b) finned heat exchanger.

Next, correlations for each exchanger geometry to fit the CFD results are proposed. For the finned-tube heat exchanger, the ethylene glycol side exhibits a laminar flow regime, while the gas side exhibits a turbulent regime. The correlations for the hot side local Nu number at a dimensionless distance of 0.5 for all configurations are presented in **Figure 20**. **Figure 21** presents the local cold side Nusselt number for a dimensionless distance of 0.45 for all configurations. The correlations have the form.

$$\text{For ethylene glycol (EG): } Nu_x = mRe^n Pr^L \quad (16)$$

$$\text{For gas (G): } Nu_x = mRe^n [(A_f/A_t)Pr]^L \quad (17)$$

In the case of the helical-tube heat exchanger, a similar correlation for the ethylene glycol was proposed. On the gas side, a factor was proposed by dividing internal diameter of the gas side over the difference of the outside diameter of the annular side minus the internal diameter of the gas side. In the same way, a

parameter ( $\delta$ ) was used. This parameter is the ratio between the helix diameter and the internal diameter of the gas side. The correlations for Nu number are presented in **Figure 22** for the hot side and **Figure 23** for the cold side for dimensionless distance of 0.7 and 0.1, respectively. The correlations have the form.

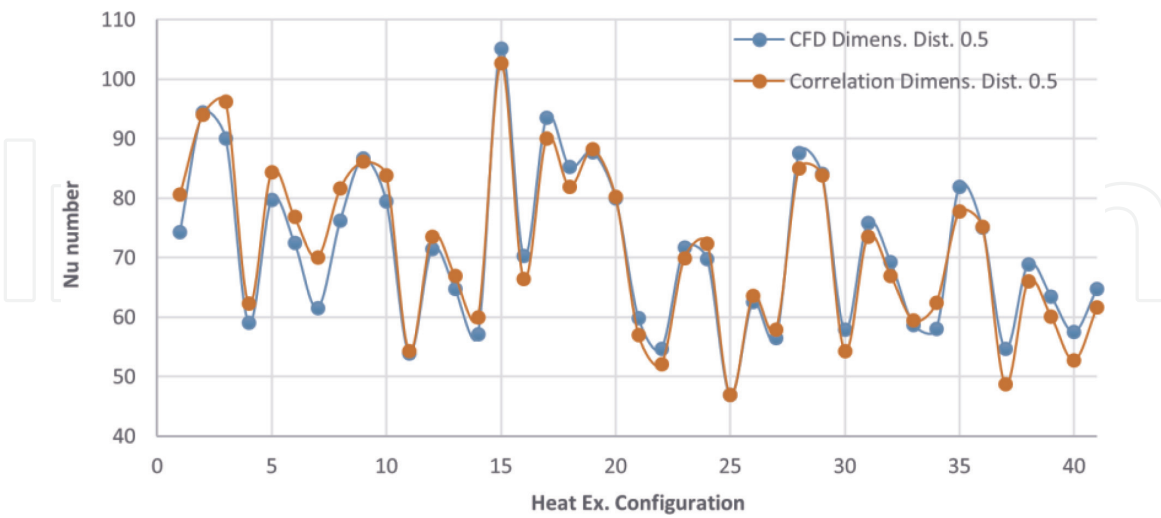


**Figure 20.**  
 Correlation for gas side (G) in the finned-tube geometry.

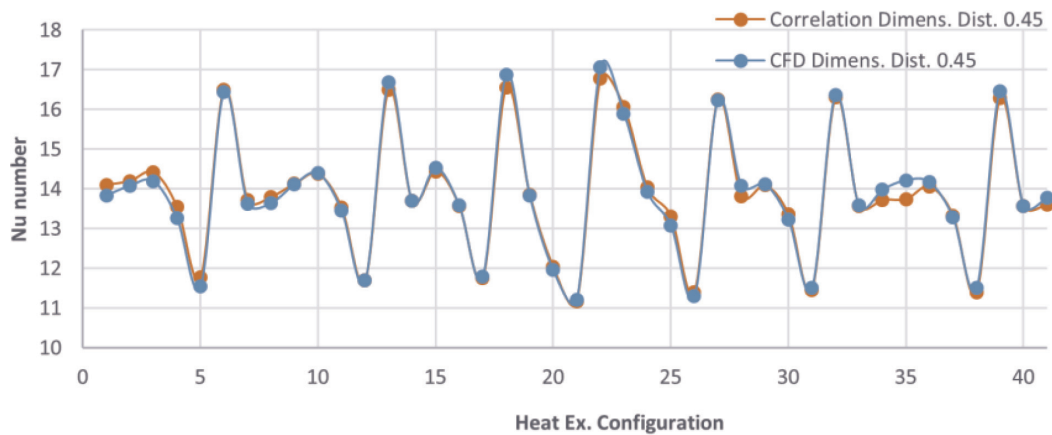


**Figure 21.**  
 Correlation for cold side (EG) in the finned-tube geometry.

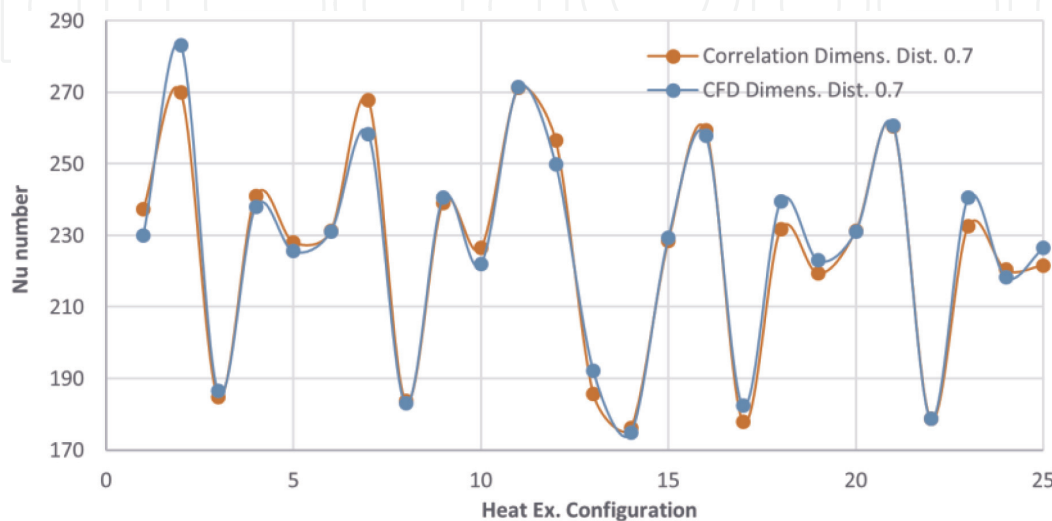


**Figure 22.**  
 Correlation for the hot side (G) of the helical-tube geometry.

$$Nu_x = mRe^n Pr^L \tag{18}$$

$$Nu_x = mRe^n [(D_i / (D_o - D_i)) (1 / (\delta))]^L \tag{19}$$

### 4.3 Neural network

An artificial neural network approach is proposed to fit the response variables of the DOE; these are the inputs given by the DOE (experiments) and CFD simulations. The object is to train the neural network using the input and the corresponding output data derived from the experimental measurements. This process is known as single training cycle or iteration. The cycle is repeated sequentially using a back-propagation algorithm so that training proceeds iteratively until the mean square error between the predicted outputs and corresponding measured values is reduced to an acceptable level. So, the results were introduced in the neural network, and the outputs of the network match very well with some results obtained from CFD. It is observed that the neural network can do a good fitting for the Nu number and heat flux for both types of heat exchangers. **Figures 24–27**

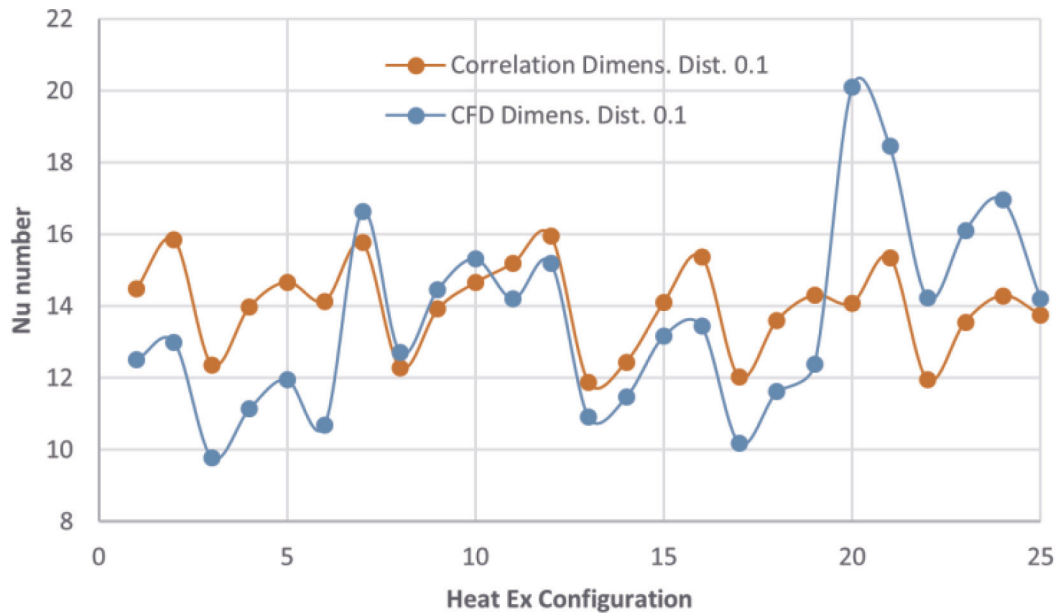


**Figure 23.** Correlation for the cold side (EG) of the helical-tube geometry.

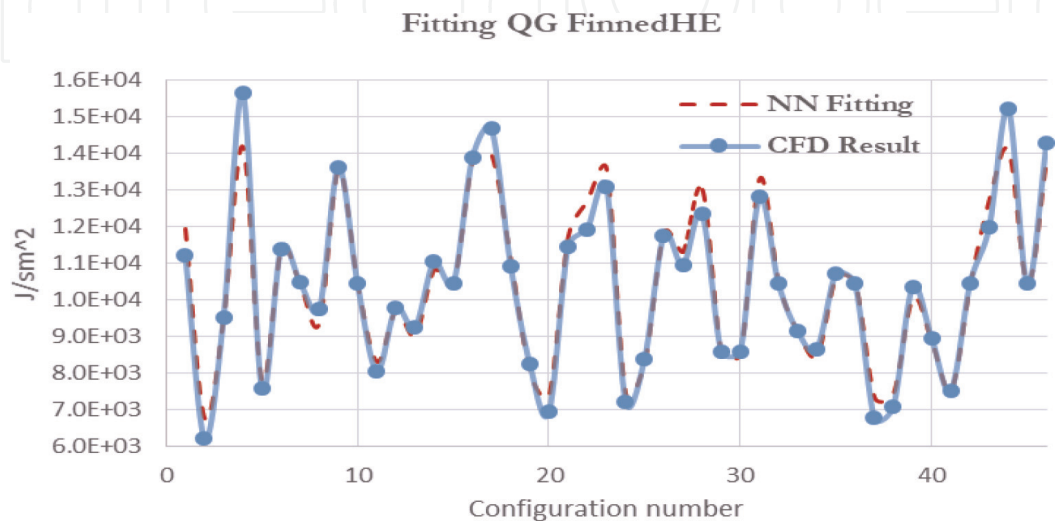


**Figure 24.** Neural network fitting for heat flux on the hot side (gas).

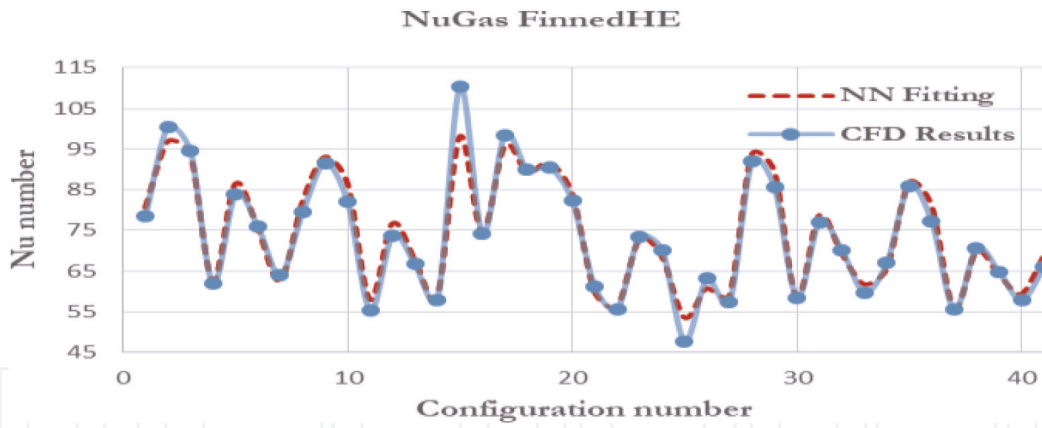


**Figure 25.** Neural network fitting for the Nu number on the hot side of the finned tube exchanger.

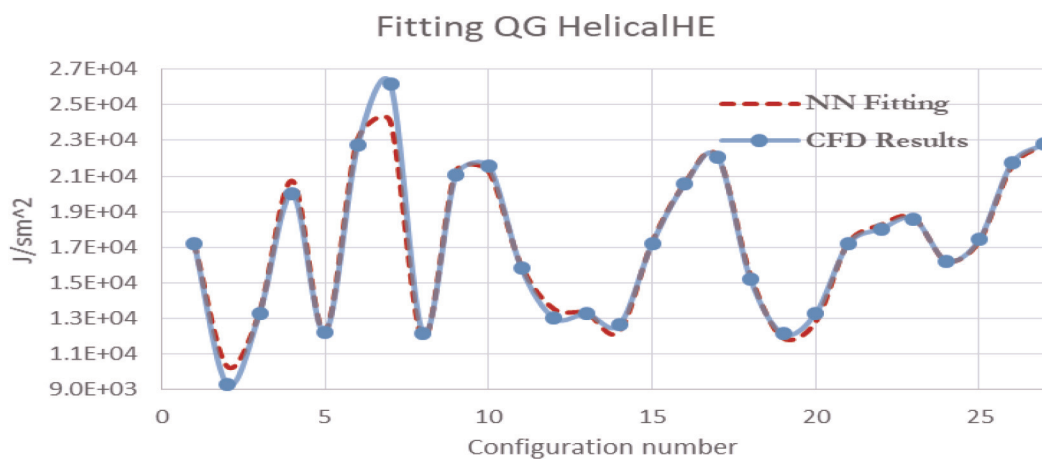


**Figure 26.** Neural network fitting for the heat flux on the hot side (gas).

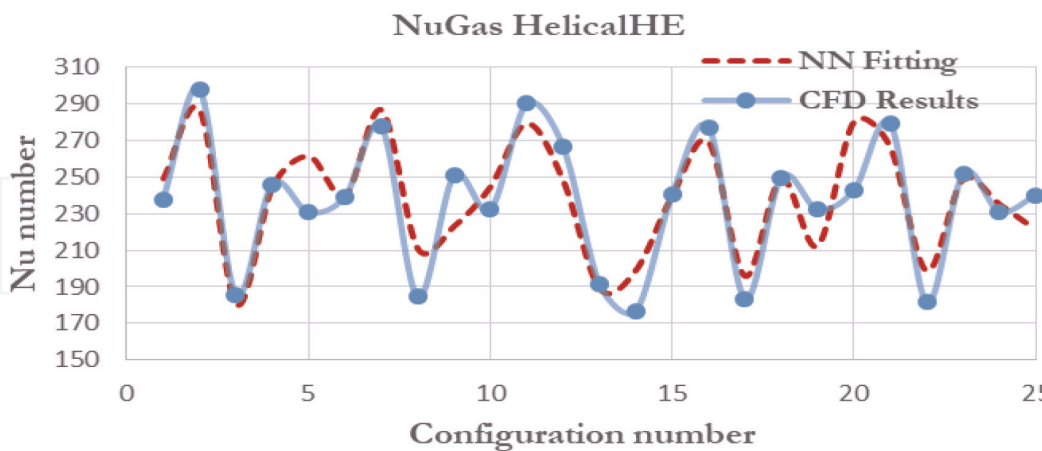


**Figure 27.** Neural network fitting for the Nu number on the hot side of the helical exchanger.

show the results of the fitting for heat flux and Nu number. NN fitting stands for neural network fitting.

#### 4.4 Exergy analysis

Exergy analysis allows to identify the components of the power cycle, whose parameters have greater influence on the maximum power generation of the

Organic Rankine Cycle. An optimization is done maximizing heat transfer and minimizing pressure drop and overheated and overcooled areas for each of the configurations simulated in CFD. **Tables 6** and **7** show the exergy analysis for each heat exchanger, where the last column shows the optimization results. From the results, it is seen that the helical heat exchanger is more efficient than the finned heat exchanger. The overheated area of the helical heat exchanger has similar values than the finned heat exchanger. The overcooled area of the helical heat exchanger is higher than the finned heat exchanger. Pressure drop for the ethylene glycol side for both types of heat exchanger has similar values. The same variable for the gas side is higher in the helical exchanger than in the finned exchanger. Finally, the heat transfer is higher in the helical heat exchanger than in the finned heat exchanger. The heat exchanger has similar dimensions, so it could be a good idea to use a helical heat exchanger to extract as much heat as possible. The pressure drop could be an important factor to consider as well. In that case, the finned heat exchanger could be considered.

	Conf 5	Conf 10	Conf 12	Conf 14	Conf 24	Helical O
Temp in gas [K]	700.0	700.0	700.0	700.0	700.0	700.0
Temp out gas [K]	582.4	559.2	591.0	514.3	545.8	560.6
Temp in EG [K]	300.0	300.0	300.0	300.0	300.0	300.0
Temp out EG [K]	389.9	406.2	391.7	409.9	415.6	404.0
$\Delta P$ gas [Pa]	3406.0	1806.4	3308.7	664.0	1062.7	882.9
$\Delta P$ EG [Pa]	5.7	24.0	17.5	9.3	45.2	25.2
Q gas [J/s]	-17011.3	-20296.6	-23368.1	-13803.7	-22188.2	-17717.6
Q EG [J/s]	16870.0	20086.6	22958.2	13880.6	21954.8	18076.9
Overheated area [%]	0.629	2.27	0.892	4.59	4.659	11.725
Overcooled area [%]	92.407	80.023	89.209	69.046	70.194	4.164
Second law effect [%]	22.7	27.2	22.7	29.9	29.7	9.9

**Table 6.**  
*Exergy balance for the helical-tube geometry.*

	Conf. 20	Conf. 22	Conf. 24	Conf. 27	Conf. 37	Conf. 39	Finned O
Temp in gas [K]	700.0	700.0	625.0	700.0	625.0	700.0	697.0
Temp out gas [K]	605.9	575.8	542.7	584.2	520.5	590.4	617.8
Temp in EG [K]	300.0	300.0	300.0	300.0	300.0	300.0	300.0
Temp out EG [K]	319.6	337.0	317.1	330.2	331.1	328.5	320.5
$\Delta P$ gas [Pa]	318.6	107.8	443.7	324.1	131.0	271.7	109.1
$\Delta P$ EG [Pa]	56.7	18.4	59.3	31.6	19.3	31.9	42.1
Q gas [J/s]	-10111.7	-6647.4	-8680.5	-9303.4	-5498.7	-8815.0	-7662.0
Q EG [J/s]	9506.9	6321.3	8306.3	8811.6	5306.4	8336.1	7199.5
Overheated area [%]	0.52	0.764	1.277	0.322	0.961	0.481	1.066
Overcooled area [%]	26.4	27.601	9.623	44.097	6.839	37.083	9.53
Second law effect [%]	5.4	10.3	5.4	8.4	9.9	7.9	2.1

**Table 7.**  
*Exergy balance for the finned-tube geometry.*

	Optimized	24	12
Mass [kg]	0.069	0.075	0.1
Temp [K]	404	415.6	391.7
Temp[°C]	130.85	142.45	118.55
$W_{in}$ [kJ/s]	1.20E-02	1.44E-02	1.53E-02
$W_{out}$ [kJ/s]	1.137	1.364	1.447
Eff %	6.28	6.21	6.3

**Table 8.**  
 Power output using the helical-tube heat exchanger.

	Optimized	22	20
Mass [kg]	0.145	0.07	0.2
Temp [K]	321	337	319
Temp[°C]	47	59	45.85
$W_{in}$ [kJ/s]	6.34E-03	4.15E-03	8.08E-03
$W_{out}$ [kJ/s]	0.5994	0.3927	0.7647
Eff %	8.33	6.21	8.04

**Table 9.**  
 Power output using the finned-tube heat exchanger.

#### 4.5 Power production

The commercial software Aspen HYSYS [11] is used to simulate an ORC thermodynamic cycle to determine the power obtained considering the operating conditions of the cycle. To determine the convenience of recovering heat from the combustion gases, it is essential to determine how much heat can be recovered. The output of the simulation model provides the maximum power obtained from the ORC. Butane is used as the working fluid and ethylene glycol as the heating fluid. Two of the best configurations and the optimized case were taken from each of the heat exchanger geometries. Configurations 12 and 24 were used for the case of the helical-tube heat exchanger and configurations 20 and 22 for the case of the finned-tube heat exchanger.

The results indicate that more power can be produced if the helical heat exchanger is used for the exhaust gas heat recovery. **Tables 8** and **9** show the results of the simulation of the Organic Rankine Cycle.

#### 5. Conclusions

This work has introduced a methodology compounded of various techniques of analysis to solve a complex problem: to maximize the power production obtained through the operation of an Organic Rankine Cycle using the heat recovered from the exhaust gases of a diesel engine. Further complexity was imposed since the heat exchangers were required to fit in a fixed length dimension. Operating variables that need to be carefully maintained are heat exchanger pressure drop on the hot side to avoid operating problems in the engine; overheated and overcooled areas in

the heat exchanger to avoid either evaporation of the cold fluid or condensation on the gas side. The approach followed to achieve the objective was composed of a set of tools such as design of experiments, computational fluid dynamics, artificial neural networks, exergy analysis, and process simulation. All these tools were required at some point of the design methodology. Although the overall approach seems to be rather complex and elaborated, it guided the results to the established objective. Two different types of heat exchanger technology were analyzed, resulting that for the objective of the design, the helical-tube heat exchanger, apart from fulfilling all the restrictions cited above, it also provides the larger power generation.

In terms of the results, additional conclusions can be drawn:

1. The optimized configuration for both types of heat exchangers does not exhibit the highest second law efficiency. This is so since several variables were considered in the optimization process, not only the heat transfer. The heat flux is maximized, but at the same time, the pressure drop and the overheated and overcooled areas are minimized.
2. A good prediction was obtained in the case of QG” and QEG” for the finned-tubed heat exchanger. This result is very important because the neural network could predict the complex behavior of the DOE and CFD results. This is so for three variables: Nu Gas, QG”, and QEG” for the finned-tube geometry.
3. The power output obtained is in the order of 0.39 to 1.446 kW. So, this energy could be used to run several devices. An economic study is needed to determine the heat recovery rate at which the operation of a power generating engine becomes affordable.

## Author details

Armando Gallegos-Muñoz<sup>1\*</sup>, Fabián Luna-Cabrera<sup>1</sup>, Martín Picón-Núñez<sup>2</sup>, Francisco Elizalde-Blancas<sup>1</sup> and Juan Manuel Belman-Flores<sup>1</sup>

<sup>1</sup> Department of Mechanical Engineering, University of Guanajuato, Salamanca, Gto, México

<sup>2</sup> Department of Chemical Engineering, University of Guanajuato, Salamanca, Gto, México

\*Address all correspondence to: gallegos@ugto.mx

## IntechOpen

© 2019 The Author(s). Licensee IntechOpen. This chapter is distributed under the terms of the Creative Commons Attribution License (<http://creativecommons.org/licenses/by/3.0>), which permits unrestricted use, distribution, and reproduction in any medium, provided the original work is properly cited. 

## References

- [1] Hatami M, Ganji D, Gorji-Bandpy M. A review of different heat exchangers designs for increasing the diesel exhaust waste heat recovery. *Renewable and Sustainable Energy Reviews*. 2014;**37**: 168-181. DOI: 10.1016/j.rser.2014.05.00450
- [2] Hatami M, Jafaryar M, Ganji D, Gorji-Bandpy M. Optimization of finned-tube heat exchangers for diesel exhaust waste heat recovery using CFD and CCD techniques. *International Communications in Heat and Mass Transfer*. 2014;**57**:254-263. DOI: 10.1016/j.icheatmasstransfer.2014.08.015
- [3] Bari S, Hossain S. Design and optimization of compact heat exchangers to be retrofitted into a vehicle for heat recovery from a diesel engine. *Procedia Engineering*. 2015;**105**: 472-479. DOI: 10.1016/j.proeng.2015.05.077
- [4] Bari S, Hossain SN. Waste heat recovery from a diesel engine using shell and tube heat exchanger. *Applied Thermal Engineering*. 2013;**61**:355-363. DOI: 10.1016/j.applthermaleng.2013.08.02
- [5] Tan C, Ward J, Wilcox S, Payne R. Artificial neural network modelling of the thermal performance of a compact heat exchanger. *Applied Thermal Engineering*. 2009;**29**:3609-3617. DOI: 10.1016/j.applthermaleng.2009.06.017
- [6] Shivakumar KM, Srinivasa Pai P, Shrinivasa Rao BR. Application of neural networks for the prediction of heat transfer parameters in a multi pass cross flow heat exchanger. In: *Proceedings of the 3rd World Conference on Applied Sciences, Engineering & Technology*. Kathmandu, Nepal; 27–29 September 2014
- [7] Hatami M, Ganji D, Gorji-Bandpy M. Experimental and numerical analysis of the optimized finned-tube heat exchanger for OM314 diesel exhaust exergy recovery. *Energy Conversion and Management*. 2015;**97**:26-41. DOI: 10.1016/j.enconman.2015.03.032
- [8] Aly WI. Computational fluid dynamics and optimization of flow and heat transfer in coiled tube-in-tube heat exchangers under turbulent flow conditions. *Journal of Thermal Science and Engineering Applications*. 2014; **6**(3):031001. DOI: 10.1115/1.4026120
- [9] Hossain SN, Bari S. Waste heat recovery from the exhaust of a diesel generator using Rankine cycle. *Energy Conversion and Management*. 2013;**75**: 141-151. DOI: 10.1016/j.enconman.2013.06.009
- [10] Fabián LC. Methodology to design heat exchangers with limited space using engine exhaust gases to generate power [Thesis]. Salamanca, Gto: Guanajuato University; 2017
- [11] Aspen Hysys. V10. USA: Aspen Technology, Inc. Available from: <https://www.aspentech.com/en/whats-new-in-v10>
- [12] Minitab 17 Statistical Software [Computer Software]. State College, PA: Minitab, Inc; 2010. Available from: [www.minitab.com](http://www.minitab.com)
- [13] Mathews PG. *Design of Experiments with MINITAB*. New Dehli: New Age; 2010
- [14] Ansys-Fluent, Release 16.0. Available from: [www.ansys.com/.../ansys-fluent-benchmarks-release-16](http://www.ansys.com/.../ansys-fluent-benchmarks-release-16)
- [15] Salim MS, Cheah SC. Wall  $y^+$  strategy for dealing with wall-bounded turbulent flows. In: *Proceedings of the*

International Multi Conference of  
Engineers and Computer Scientists  
(IMECS 2009). Hong Kong; 18-20  
March 2009

[16] Ansys Fluent. Choosing the  
Pressure-Velocity Coupling Method.  
Retrieve from: [https://www.sharcnet.ca/  
Software/Fluent6/html/ug/  
node1021.htm](https://www.sharcnet.ca/Software/Fluent6/html/ug/node1021.htm)

[17] Cyklis P, Młynarczyk P. The  
influence of the spatial discretization  
methods on the nozzle impulse flow  
simulation results. *Procedia  
Engineering*. 2016;**157**:396-403. DOI:  
10.1016/j.proeng.2016.08.382

[18] Ansys Fluent. Spatial Discretization.  
Retrieved from: [http://www.afs.enea.it/  
project/neptunius/docs/fluent/html/th/  
node366.htm](http://www.afs.enea.it/project/neptunius/docs/fluent/html/th/node366.htm)